Far-Field Optical Imaging and Manipulation of Individual Spins with Nanoscale Resolution

Far-field optical imaging and manipulation of individual spins with nanoscale resolution

P. C. Maurer[1,*], J. R. Maze[1,7,*], P. L. Stanwix[2,8,*], L. Jiang[6], A.V. Gorshkov[1], A.A. Zibrov[1], B. Harke[3], J.S. Hodges[1,4], A.S. Zibrov[1], A. Yacoby[1], D. Twitchen[5], S.W. Hell[3], R.L. Walsworth[1,2], M.D. Lukin[1]

[1]*Department of Physics, Harvard University, Cambridge, Massachusetts 02138 USA*

[2]*Harvard-Smithsonian Center for Astrophysics, Cambridge, Massachusetts 02138 USA*

[3]*Max Planck Institute for Biophysical Chemistry, Gottingen, Germany.*

[4]*Department of Nuclear Science and Engineering, Massachusetts Institute of Technology, Cambridge, Massachusetts 02139, USA*

[5]*Element Six Ltd, Ascot, Berkshire, UK.*

[6]*Institute for Quantum Information, California Institute of Technology, Pasadena, CA 91125, USA.*

[7]*Facultad de Física, Pontificia Universidad Católica de Chile, Casilla 306, Santiago, Chile.*

[8]*School of Physics, University of Western Australia, Crawley, Western Australia 6009, Australia.*

[*]These authors contributed equally to this work.

A fundamental limit to existing optical techniques for measurement and manipulation of spin degrees of freedom is set by diffraction, which does not allow spins separated by less than about a quarter of a micrometer to be resolved using conventional far-field optics. Here, we report an efficient far-field optical technique that overcomes the limiting role of diffrac-

tion, allowing individual electronic spins to be detected, imaged and manipulated coherently with nanoscale resolution. The technique involves selective flipping of the orientation of individual spins, associated with Nitrogen-Vacancy (NV) centers in room temperature diamond, using a focused beam of light with intensity vanishing at a controllable location, which enables simultaneous single-spin imaging and magnetometry at the nanoscale with considerably less power than conventional techniques. Furthermore, by inhibiting spin transitions away from the laser intensity null, selective coherent rotation of individual spins is realized. This technique can be extended to sub-nanometer dimensions, thus enabling applications in diverse areas ranging from quantum information science to bioimaging.

Optical techniques constitute powerful tools for spin detection and manipulation that enable applications ranging from atomic clocks[1,2] and magnetometers[3], to quantum information processors[4–7] and novel sensors and imaging modalities for biological and life sciences[8–13]. Several promising methods for fluorescence imaging have recently been developed to surpass the diffraction limit and are already being applied to important problems in biology and neuroscience[14–16] as well as sub-wavelength optical lithography[17–19]. For example, sub-diffraction imaging of fluorophores can be obtained by stimulated emission depletion (STED) microscopy and related methods based on reversible saturable optical linear fluorescence transitions (RESOLFT)[20–23]. Using optical fields with intensity zeros and steep spatial gradients, such as those provided by doughnut-shaped beams, one can transiently switch the fluorophores to a different state everywhere except for a small region near the vanishing optical intensity. In this case the emitters from that small region can be separated from neighbours closer than the diffraction limit. Since the emitters are

switched to the designated (on or off) state provided the optical stimulation rate exceeds that of the spontaneous decay rate of that state, the ultimate resolution is, in principle, limited only by the applicable optical power[23].

The concept of sub-diffraction spin detection and control

Our new approach to sub-diffraction spin detection and manipulation is outlined in Figure 1. We consider an electronic spin system, such as the NV center in diamond, which can be polarized via optical pumping, coherently manipulated with resonant microwave radiation, and read-out with spin-state-dependent fluorescence. Improved spatial resolution is achieved by illuminating the sample with a doughnut-shaped optical beam just prior to optical spin readout. Spins positioned directly in the center of the doughnut beam are not affected by it. However, spins that are even a few tens of nanometers away from the zero intensity position are re-polarized by the doughnut beam and thus contribute differently to the fluorescence signal, providing nanoscale imaging contrast. Moreover, selective coherent manipulation of a spin in the doughnut center can be achieved by simultaneous exposure to resonant microwave radiation and the optical doughnut beam (Figure 1c). The essence of this process is that all coherent spin transitions away from the doughnut center are inhibited by the laser field, thereby allowing coherent rotation of an individual spin at the doughnut center.

Before proceeding we note that STED and related RESOLFT techniques have been demonstrated to be effective in systems containing metastable states[20], but in all cases electronic excitations were critically employed to resolve at sub-diffraction distances. A specific advantage of

our present approach, which we refer to as spin-RESOLFT, stems from the exceptionally long lifetimes associated with spin sublevels of electronic ground states in certain systems, which can reach seconds and exceed the lifetimes of electronic transitions by more than six orders of magnitude. Optical transitions involving such ground-state spin levels can be differentially saturated by scattering just a few photons. Therefore, spin-RESOLFT allows individual electronic spins associated with NV centers to be imaged on the nanoscale, with several orders of magnitude lower laser power than most other super-resolution imaging techniques. This offers significant advantages in many applications, especially to biological systems. Alternatively, for a given power of the doughnut laser beam, spin-RESOLFT allows a dramatic improvement in resolution relative to STED and other RESOLFT approaches, potentially extending to sub-nanometer scales. We also note that another method for resolving closely spaced spins employs large magnetic field gradients[12], as in conventional magnetic resonance imaging. This method, however, requires detailed knowledge of the magnetic gradient topography and is only possible for spins that can be resolved spectrally in ESR or NMR measurements. In what follows we show that the present technique allows one to use far-field optical detection to resolve individual spins spaced by sub-diffraction distances, sense their local magnetic environment, and perform coherent spin manipulation, even when ESR or NMR measurements are not capable of resolving individual spins spectrally.

Nanoscale optical imaging using spin state

Our experimental demonstration makes use of individual NV centers in diamond. An electronic spin associated with the NV triplet ground state can be optically polarized, coherently ma-

nipulated using conventional electron spin resonance (ESR) techniques[24,25], and read-out through spin-state-dependent fluorescence[26] (see Figure 1b). NV centers in ultra pure diamond display exceptional electron spin lifetimes (T_1), approaching seconds at room temperature[5,13]. To realize sub-diffraction optical imaging and magnetometry using NV spins, we first polarize all NV centers in the field of view into the ground spin state $m_s = 0$ using a focused Gaussian beam; then drive ESR spin transitions to the $m_s = +1$ or -1 state, or to a coherent superposition of these states; and subsequently use an optical doughnut beam to selectively re-polarize the spins of nearby NV centers. NV centers located in regions of high intensity are optically pumped to the $|0\rangle$ ground state, whereas an NV center located at the central intensity zero remains unaffected and maintains its original state. Thus, spatial information associated with this central NV is encoded into its electronic spin state. It is subsequently determined by conventional optical readout of the NV fluorescence, since the NV centers that are not repolarized are darker than those that are repolarized. Scanning the sample with respect to the beams and repeating the above procedure allows sub-diffraction imaging of the NV centers in the field of view, as well as sensitive nanoscale magnetometry at the location of each NV center due to the Larmor precession of a coherent superposition of NV spin states (detectable via spin-state-dependent fluorescence)[9,10].

Figure 2 shows example sub-diffraction optical images of an NV electronic spin in diamond, acquired using the spin-RESOLFT technique. A ten-fold improvement of 1D resolution was obtained for a fixed power of approximately 2 mW, focused to a diffraction limited spot of 0.07 μm^2, by increasing the duration of the doughnut beam pulse. A similar resolution improvement was achieved for much lower doughnut power of about 0.1 mW, provided the decrease in power is

compensated by an increase in doughnut duration. These observations are in excellent agreement with predictions from a simple model of the imaging resolution Δr provided by our sub-diffraction spin detection technique (see Methods and SI):

$$\Delta r \approx \frac{\lambda/2\mathrm{NA}}{\sqrt{1+\Gamma t_D}} \tag{1}$$

Here λ is the wavelength of the optical field, NA is the numerical aperture of the objective, Γ characterizes the maximum rate of optical excitation out of spin state $|1\rangle$, and t_D is the duration of the doughnut beam. Note that the spin imaging resolution is determined by the product of the power and duration of the doughnut beam: hence sub-diffraction-limited resolution can be achieved with a laser power that is well below optical saturation of the excited state (^3E), provided that t_D is sufficiently long. Since the maximum length of t_D is limited by spin state relaxation ($T_1 > 100$ ms) for spin-RESOLFT and by the electronic excited state lifetime ($\sim$10 ns) for STED, we are able to realize sub-diffraction spin imaging using sub-mW doughnut beam power with comparable resolution to that of STED using about one Watt of doughnut power[23].

Sub-wavelength optical magnetometry

To demonstrate simultaneous nanoscale spin imaging and magnetometry, we applied the spin-RESOLFT technique to NV centers in bulk diamond separated by less than the diffraction limit. Figure 3a shows sub-diffraction 2D imaging of two NV centers with identical ESR lines. In this case, it is not possible to identify the presence of multiple centers using conventional confocal imaging and ESR techniques alone. However, by using our new technique, the presence of two

NV centers separated by $\sim$150 nm is directly revealed in a 2D sub-diffraction spin image (Figure 3b).

Detection of local magnetic fields with sub-diffraction resolution is presented in Figures 3c,d. Specifically, when imaged individually with spin-RESOLFT, each NV center exhibits a distinct modulation of its Rabi oscillation (Figure 3c), determined by a relative shift in the center's ESR transition frequency arising from small differences (< 1 G) in the static local magnetic field that each center experiences. Even more subtle differences in the local magnetic field environment of the two NV centers are revealed by sub-diffraction spin-echo measurements using spin-RESOLFT (Figure 3d). While at short times each of the centers display spin echoes modulated by Larmor precession of the ^{15}N nuclei in the applied static magnetic field, at longer times the echo signals are substantially different. Center 2 displays good coherent dynamics, evidenced by echo revivals exceeding 20 μs, whereas Center 1 shows no echo revival, due to a nearby ^{13}C nucleus[27] or other magnetic defects (see Methods and SI). When NV centers have different crystallographic axes and therefore different ESR spectra, the spin-RESOLFT technique can associate each spectral line with the corresponding location of an individual NV centers with sub-diffraction limited resolution (see Figure S1 in Methods and SI).

Coherent spin control

The spin-RESOLFT technique also enables selective coherent manipulation of individual NV spins separated from other nearby NV centers by less than the diffraction limit. Applying a strong optical doughnut field simultaneously with a resonant microwave field (Figure 4a) can

suppress coherent spin transitions away from the laser intensity null.

We first demonstrated this effect for an individual, isolated NV center, initially polarized into its $m_s = 0$ state. To distinguish the optical suppression of microwave-driven spin transitions from the conventional optical process used above for re-polarization, we exploited the fact that the optical pumping from $m_s = \pm 1$ into $m_s = 0$ occurs via transition through a metastable singlet state on a timescale of about $\tau_s = 300$ ns. Therefore, we applied a microwave π pulse driving the $|0\rangle \rightarrow |1\rangle$ transition together with a simultaneous pulse of the green laser beam; after which we immediately (within $\tau_d \leq 50$ ns $\ll \tau_s$) optically measured the populations in the $m_s = 0, \pm 1$ and metastable singlet states (see SI). As shown in Figure 4a, as we increased the laser power, the population in each state (triangles) approached the values measured when no microwave pulse was applied (open circles). This demonstrates that at high laser power no population transfer occurs between the $|0\rangle$ and $|1\rangle$ states. Since our experiment measured the populations before the metastable singlet could decay into the ground state $m_s = 0$, the data of Figure 4a directly confirms that the observed inhibition of population transfer was not due to repumping out of the $|m_s| = 1$ states.

The observed population dynamics can be due to three effects, all of which result in a suppression of coherent spin manipulation by the applied microwave field. First, if an NV center is optically promoted to the electronic excited state, then the microwave transition between spin states with $m_s = 0$ and $m_s = 1$ is suppressed due to the different zero field splitting in the electronic ground and excited states. Second, if an NV center is transferred nonradiatively to the metastable

$^1A_1$ state, then coherent spin rotations are prevented since the $^1A_1$ state is a spin singlet. Finally, optical excitation inhibits the build up of spin coherence between the $|0\rangle$ and $|1\rangle$ states even in the absence of population transfer to the excited state, a phenomena known as the quantum Zeno effect[28]. To estimate how substantially each of these three processes contributes to the observed suppression of coherent spin transitions, we calculated the populations in the electronic excited state and in the $^1A_1$ state using the transition rates determined in Figure 4a. As shown in Figure S4 in SI for our experimental parameters ($R/\gamma \approx 1$), the estimated population in the ground state is of the same order as the sum of populations in the excited state and the singlet. Thus population transfer and the quantum Zeno effect contribute approximately equally to the observed suppression of coherent spin manipulation.

We next employed spin-RESOLFT for selective coherent manipulation of one of two closely spaced NV spins (Center 1 in Figure 3b), while the other NV spin (Center 2) was kept in its $m_s = 0$ state via optically-induced suppression of coherent spin transitions, as discussed above. A pulsed strong doughnut beam was applied simultaneously with a microwave pulse of variable Rabi spin-flip angle, followed by optical measurement of the state of the NV spin at the doughnut center. In a separate calibration experiment, the states of both NV spins were measured together (no optical doughnut applied) as a function of microwave pulse length (Rabi spin-flip angle). The spin-RESOLFT and calibration measurements enabled us to determine the states of the two proximally spaced NV spins individually. Specifically, two experiments were performed. In one, the spin states of both NV centers were measured (sequence S3); in the second, the spin state of Center 1 was determined using spin-RESOLFT (sequence S4); see SI for details. As shown in Figure

4b, spin transitions are inhibited for the NV center outside the central null of the doughnut beam; whereas the central NV spin undergoes coherent evolution, i.e., Rabi oscillations, in excellent agreement with a theoretical model (blue and green curves in Figure 4b), as described in Methods and SI.

Outlook

As shown in these demonstration experiments, the far-field optical resolution for spin imaging and coherent manipulation is no longer limited by diffraction. We expect the resolution and speed of the spin-RESOLFT technique to be significantly improved by technical upgrades such as increasing the contrast between the intensity of the doughnut crest and that of the central minimum, i.e., perfecting the doughnut zero[23]. In addition, implementing relatively large values of Γt_D, where $\Gamma \sim 100$ MHz near optical saturation and t_D is on the order of the electronic spin lifetime T_1 (which ranges from 10 ms[5] to longer than a second in ultrapure diamond[13]), should allow more than a 1000 fold improvement of resolution below the diffraction barrier, making it feasible to attain sub-nanometer optical spin detection and manipulation, including sensitive measurement of magnetic fields. Finally, the low levels of light required for our technique will also facilitate the parallelization of this imaging process by replacing the scanning doughnut beam with moving arrays of lines or doughnuts of vanishing intensity. This modification should enable fast camera-based spin imaging over a large field of view.

The capability to optically detect and manipulate individual spins with sub-diffraction resolution opens the door to a number of powerful applications in both the physical and life sciences.

For example, spin-RESOLFT could be used for high fidelity addressing of individual spin qubits in an array composed from NV centers separated by distances in the range of 10-30 nm. In such a case, nearby electronic spins could be coupled directly via magnetic or optical dipole-dipole interactions, thereby enabling high fidelity two-qubit operations. By encoding qubits into nuclear spins nearby to specific NV centers, and using spin-RESOLFT for sub-diffraction addressing of electronic spins and control of electron-nuclear systems, both readout and coherent manipulation could be enabled on nanometer scales, thereby opening a new route to a room temperature scalable quantum information processor (see also [29]). More specifically, the demonstrated suppression of electronic Rabi oscillations (Figure 4b) allows for preparation, detection, and coherent manipulation of one nuclear spin (associated with the NV center in the zero of the green doughnut-shaped beam) without affecting qubits encoded in the nuclear spins of surrounding centers[30,31] (see Methods and SI). Likewise, intriguing applications in bioscience can be foreseen for spin-RESOLFT, which combines high sensitivity magnetometry with sub-diffraction imaging resolution. Examples include the use of NV-diamond nanocrystals in living cells as photostable fluorescent biomarkers and sensors of nanoscale magnetic fields, e.g., for direct imaging of activity in neuronal networks and mapping the local concentration of reactive oxygen species and intra-cellular ions. In addition, by exploiting long-lived ground electronic spin states, spin-RESOLFT has the potential for reaching extraordinary imaging and sensing resolution with modest laser power levels, which may be of interest for a diversity of super-resolution imaging applications involving, in particular, biological systems. Finally, we expect that our approach can be applicable to a wide variety of spin systems, from trapped atoms and ions to quantum dots, which may enable a diverse range of interesting

applications in quantum science and engineering.

METHODS

Samples

All described experiments were performed at room temperature on an ultrapure single crystal bulk diamond grown by chemical vapour deposition (CVD). Nitrogen vacancy (NV) centers were created by irradiating the CVD diamond with 10^9 cm^{-2} of nitrogen ions with energy of 6 keV, corresponding to an estimated average implantation depth of 10 nm, as determined by simulations. The sample was then annealed at 800 °C, yielding an observed NV concentration of approximately 0.6 NV/μm^2. To reliably distinguish shallow implanted ions from natural NV centers, a rare isotope ^{15}N was used.

Confocal and spin-RESOLFT microscopy

NV centers were probed using a custom-built confocal fluorescence microscope. Two 532 nm laser beams provided optical excitation, one a Gaussian shaped beam and the other a dough-nut shaped beam. The two beams, which could be independently switched using Acousto-Optic Modulators (AOMs - Crystal Technology and Isomet), were combined on a polarised beam splitter before entering an oil immersion objective (Nikon Plan Fluor 100x 1.3 NA). Fluorescence from the NV centers was collected back through the objective, separated from the excitation path via a

custom dichroic with high surface flatness (Chroma Technology). The fluorescence was filtered $(630 - 750)$ nm and focused onto a single-mode fibre connected to an avalanche photo detector (APD - Perkin Elmer). Imaging was achieved by scanning the diamond sample under the objective, using a digitized 3-axis piezo translation stage (Physical Instrument P-733.3CD). The doughnut shaped mode was created by passing a Gaussian beam through the center of a helical phase ramp (RPC Photonics), which adds a phase from (0 to 2π) conditional on the azimuthal position. To prevent distortion of the doughnut center due to beam focusing by the objective, the beam was circularly polarized by placing a quarter-lambda waveplate immediately before the objective.

Electronic spin manipulation

The electronic ground state of the NV center is a spin triplet state, with a zero field splitting of 2.87 GHz between $m_s = 0$ and $m_s = \pm 1$ due to the electron-electron interaction. Optical excitation with green light optically pump population from the $m_s = \pm 1$ state into the $m_s = 0$ state at a rate R. The degeneracy of the $m_s = \pm 1$ state was lifted via Zeeman splitting, induced by an external DC magnetic field as well as local magnetic fields to be detected via magnetometry pulse sequences. Moreover, by adjusting the direction of the external magnetic field, the relative ESR frequency for NV centers with different crystallographic orientations was controlled. The NV electronic spin state was coherently manipulated (for Rabi oscillations, spin echo measurements, etc.) by driving the electron spin resonance with a microwave field generated from a $20\mu m$ diameter wire placed on the surface of the diamond sample.

Spin imaging resolution

The spin-RESOLFT signal is proportional to $f(x) = n_0(x)I_G(x)$ where n_0 is the population of the $m_s = 0$ state, $I_G = \exp(-\alpha(x/r_C)^2)$ is the intensity profile of the gaussian beam used for readout of the electronic spin, $r_C = \lambda/2\mathrm{NA}$ is the confocal resolution and $\alpha = 4/log(2)$. n_0 depends on duration of the doughnut beam t_D; it can be evaluated by solving rate equations given in the SI. In the limit of large lifetime of spin transition, it is given by $n_0 = \exp(-R_x t_D)$, where R_x is the position-dependent optical polarization rate. In the unsaturated regime, $R_x = R_0 + \alpha\Gamma(x/r_C)^2$, where $\Gamma = \kappa\epsilon$ is proportional to the optical excitation rate associated with the maximal intensity of the doughnut κ, and ϵ is the branching ratio of the spin changing ($m_s = 1 \rightarrow m_s = 0$) decay relative to the total decay of the excited state. $R_0 = \epsilon\kappa_0$ is proportional to the intensity at the doughnut center and the corresponding excitation κ_0. The spin-RESOLFT resolution r is defined by $f(x) = \exp(-\alpha(x/r)^2)$. Solving for r leads to Eq. (1) in the main text. In our experiments, the resolution is limited by small imperfection of the doughnut-zero intensity. As shown in the SI, using a model that includes a back pumping processes that brings the electronic spin from the $m_s = 0$ to the $m_s = 1$ state and finite spin lifetime, we find that the improvement in resolution relative to the diffraction limit of a confocal microscope is given by $r/r_C \sim \sqrt{R_0/\Gamma}\sqrt{1 + 2\gamma_{0\rightarrow1}/R_0} \approx \sqrt{R_0/\Gamma}$, where $\gamma_{0\rightarrow1}$ is the total rate out of the electronic spin state $m_s = 0$. This estimate is in good agreement with experimental observations.

Measurements of local magnetic field environment

The observed modulations of the Rabi oscillations shown in Figure 3c reveal the different magnetic field experienced by each NV center. These modulations are caused by hyperfine-induced splitting in the NV electronic spin transition ($m_s = 0 \rightarrow 1$) associated with the ^{15}N nuclear spin ($I = \frac{1}{2}$). Such modulations appear when the microwave frequency is detuned from the central transition $\nu_0^i = \Delta + \gamma_e B^i$, where B^i is the magnetic field along the NV axis of center i , Δ is the zero-field splitting, and γ_e is the gyromagnetic ratio of the electronic spin. The modulation frequency for NV center i is thus given by (see SI) $(\nu_0^i - \nu)A/\Omega$, where ν is the microwave frequency, $A = 3.05$ MHz is the hyperfine interaction between the electronic and nuclear spin and Ω is the Rabi frequency. The difference in the beating frequencies of each center reveals a difference in effective static magnetic field experienced by each center of about 1 G.

In our spin echo measurements (Figure 3d), the dominant contribution comes from the interaction between the electronic spin of the NV center and the ^{15}N nuclear spin and ^{13}C nuclear spin bath. The high frequency oscillations (3.05 MHz) correspond to the hyperfine interaction A between the electronic spin and nuclear spin of the ^{15}N atom in the NV center, as discussed above. Meanwhile the slow frequency component of the dynamics (360 kHz) corresponds to the Larmor frequency of the ^{15}N nuclear spin in the local magnetic field which is enhanced by virtual transitions of the electronic and nuclear spin (SI). The enhancement factor can be as large as $2(\gamma_e/\gamma_n)(A/\Delta) \approx 14$ when the magnetic field is perpendicular to the NV axis. The observed spin echo collapses and revivals are due to the interaction between NV centers and ^{13}C nuclei. The revival frequency in Figure 3d, 74 kHz, is given by the bare Larmor frequency of ^{13}C corresponding to a magnetic field of 69 G (SI). Note that Center 1 shows no revival which is likely due to a

proximal ^{13}C nuclear spins that quickly decoheres the electronic spin of this center [23].

Coherent single spin manipulation

We performed selective coherent spin manipulation on two NV centers with a spatial separation of approximately 150 nm. To verify that Center 1 can undergo coherent Rabi oscillations while Center 2 is kept in the $m_s = 0$ state, two experiments using pulse sequences S3 and S4 in Figure 4 were performed. If Center 2 remains in the $m_s = 0$ state, a constant signal is expected for the difference of the measurements made with these sequences.

In this subtraction procedure we accounted for contrast reduction in the spin-RESOLFT readout of Center 1 by multiplying the results of sequence S4 by $\frac{1}{0.75}$. (This weighting factor is determined from a separate experiment, in which both centers were prepared in the state $m_s = 1$ and imaged with spin-RESOLFT). The signals were normalized relative to the unperturbed Rabi oscillation signal for Center 1.

The observed sub-diffraction suppression of coherent spin transitions can be used to manipulate quantum information stored in the nuclear spins associated with each NV center. Specifically, we can use this sub-diffraction inhibition to prepare, coherently manipulate, and detect the nuclear spin of Center 1 (in the doughnut center) without perturbing the nuclear spins of Center 2 and of other nearby centers. As explained in detail in the Supplementary Information, the error induced on the nuclear spin associated with Center 2 during a π-pulse on Center 1 can be estimated from our measurements as $P_e \approx \left(\frac{\gamma}{\kappa+\gamma}\right)\left(\frac{\pi\Omega}{2\kappa}\right)$, where κ is evaluated at Center 2 and where $\gamma \approx \frac{1}{13ns}$

is the decay rate of the optically excited state. In addition to the dephasing described above, this takes into account the fact that application of the green doughnut beam "hides" some population in the excited state. For values of $\kappa \sim \gamma$ and $\Omega = (2\pi)2.3$ MHz, this error would be $p_e \approx 0.1 \ll 1$, indicating that the state of the nuclear spin associated with Center 2 can be well preserved while we manipulate Center 1.

1. Jacques Vanier, C. A. The quantum physics of atomic frequency standards. (Hilger, Philadelphia, 1989).

2. Cundiff, S. T. , Ye, J. . Colloquium: Femtosecond optical frequency combs. *Rev. Mod. Phys.* **75**, 325-342 (2003).

3. Budker, D. , Romalis, M. Optical magnetometry. *Nat. Phys.* **3**, 227-234 (2007).

4. Xu, X. D. et al. Coherent Optical Spectroscopy of a Strongly Driven Quantum Dot. *Science* **317**, 929-932 (2007).

5. Dutt, M. V. G. et al. Quantum Register Based on Individual Electronic and Nuclear Spin Qubits in Diamond *Science* **316**, 1312-1316 (2007).

6. Hennessy, K. et al. Quantum nature of a strongly coupled single quantum dotcavity system. *Nature* **445**, 896-899 (2007).

7. Neumann, P. et al. Multipartite Entanglement Among Single Spins in Diamond. *Science* **320**, 1326-1329 (2008).

8. Chernobrod, B. M., Berman, G. P. Spin microscope based on optically detected magnetic resonance. *J. Appl. Phys.* **97**, 014903 (2005).

9. Taylor, J. M. et al. High-sensitivity diamond magnetometer with nanoscale resolution. *Nat. Phys.* **4**, 810-816 (2008).

10. Maze, J. R. et al. Nanoscale magnetic sensing with an individual electronic spin in diamond. *Nature* **455**, 644-647 (2008).

11. Degen, C. L. Scanning magnetic field microscope with a diamond single-spin sensor. *Appl. Phys. Lett.* **92**, 243111 (2008).

12. Balasubramanian, G. et al. Nanoscale imaging magnetometry with diamond spins under ambient conditions. *Nature* **455**, 648-651 (2008).

13. Balasubramanian, G. et al. Ultralong spin coherence time in isotopically engineered diamond. *Nature Mater.* **8**, 383-387 (2009).

14. Westphal, V. et al. Video-Rate Far-Field Optical Nanoscopy Dissects Synaptic Vesicle Movement. *Science* **320**, 246-249 (2008).

15. Zhuang, X. Nano-imaging with STORM. *Nat. Photonics* **3**, 365-367 (2009).

16. Betzig, E. et al. Imaging Intracellular Fluorescent Proteins at Nanometer Resolution. *Science* **313**, 1642-1645 (2006).

17. Li, L. J., Gattass, R. R. , Gershgoren, E., Hwang, H., Fourkas, J. T. Achieving /20 Resolution by One-Color Initiation and Deactivation of Polymerization. *Science* **324**, 910-913 (2009).

18. Scott, T. F., Kowalski, B. A., Sullivan, A. C., Bowman, C. N., McLeod, R. R. Two-Color Single-Photon Photoinitiation and Photoinhibition for Subdiffraction Photolithography. *Science* **324**, 913-917 (2009).

19. Johnson, K. S. et al. Localization of Metastable Atom Beams with Optical Standing Waves: Nanolithography at the Heisenberg Limit. *Science* **280**, 1583-1586 (1998).

20. Hell, S. W. , Wichmann, J. Breaking the diffraction resolution limit by stimulated emission: stimulated-emission-depletion fluorescence microscopy. *Opt. Lett.* **19**, 780-782 (1994).

21. Hell, S. W. Far-Field Optical Nanoscopy. *Science* **316**, 1153-1158 (2007).

22. Hell, S. W, Kroug, M. Ground-state-depletion fluorscence microscopy: A concept for breaking the diffraction resolution limit. *Appl. Phys. B* **60**, 495-497 (1995).

23. Rittweger, E., Han, K. Y., Irvine, S. E., Eggeling, C., Hell, S. W. STED microscopy reveals crystal colour centres with nanometric resolution. *Nat. Photonics* **3**, 144-147 (2009).

24. Hanson, R., Awschalom, D. D. Coherent manipulation of single spins in semiconductors. *Nature* **453**, 1043-1049 (2008).

25. Hanson, R., Dobrovitski, V. V. , Feiguin, A. E., Gywat, O. , Awschalom, D. D. Coherent Dynamics of a Single Spin Interacting with an Adjustable Spin Bath. *Science* **320**, 352-255 (2008).

26. Wrachtrup, J., Jelezko, F. Processing quantum information in diamond. *J. Phys. Condens. Matter* **18**, S807-S824 (2006).

27. Maze, J. R., Taylor, J. M., Lukin, M. D. Electron spin decoherence of single nitrogen-vacancy defects in diamond. *Phys. Rev. B* **78**, 094303 (2008).

28. Itano, W. M., Heinzen, D. J., Bollinger, J. J., and Wineland, D. J. Quantum Zeno effect. *Phys. Rev. A* **41**, 2295 (1990).

29. Gorshkov, A. V., Jiang, L., Greiner, M., Zoller, P., Lukin, M. D. Coherent Quantum Optical Control with Subwavelength Resolution. *Phys. Rev. Lett.* **100**, 093005 (2008).

30. Neumann, P., Beck, J., Steiner, M., Rathgen, H., Hemmer, P. R., Wrachtrup, J. and Jelezko, F. Quantum non-demolition measurement of a single nuclear spin. *submitted for publication*.

31. Jiang, L. et al. Coherence of an Optically Illuminated Single Nuclear Spin Qubit. *Phys. Rev. Lett.* **100**, 073001 (2008).

32. Manson, N. B., Harrison, J. P., and Sellars, M. J. Nitrogen-vacancy center in diamond: Model of the electronic structure and associated dynamics. *Phys. Rev. B* **74**, 104303 (2006).

Supplementary Information is linked to the online version of the paper at www.nature.com/nature.

Acknowledgements We gratefully acknowledge P. Cappellaro, Y. Chu, S. Folling, M. Greiner, P. Hemmer, E. Rittweger, B. Shields, E. Togan, A. Trifonov and D. Wildanger for valuable discussions and technical assistance. This work was supported by the NSF, DARPA, the Packard Foundation, the Smithsonian Institution and Harvard CNS.

Authors Contribution All authors contributed to all aspects of this work.

Competing Interests The authors declare that they have no competing financial interests.

Correspondence Correspondence and requests for materials should be addressed to lukin@fas.harvard.edu

Figure 1 Principles of sub-diffraction far-field optical imaging and magnetometry of individual NV electronic spins in diamond ("spin-RESOLFT"). **a**, Experimental sequence using pulsed optical and microwave excitation. NV spins are first optically pumped to $m_s = 0$ using a Gaussian beam at 532 nm followed by microwave manipulation. Application of 532 nm doughnut beam re-polarizes the outer ring to $m_s = 0$, allowing the spin-state of the central dark region to be independently read-out. **b**, Energy level diagram of NV center showing optical absorption (k) and fluorescence (γ) rates. NV electronic spins are optically pumped from $|m_s| = 1$ to $m_s = 0$ spin states through non-radiative relaxation via the metastable $^1A_1$ singlet state. Microwave fields at around 2.87 GHz coherently manipulate the NV spin states. The differential spin-state population is measured via spin-state-dependent fluorescence in the red. **c**, Schematic of experimental approach. NV centers are imaged using confocal microscopy by scanning the sample around the focal point using a 3-axis piezo stage. The doughnut beam is generated by passing a Gaussian beam through a vortex waveplate (2π azimuthally varying phase ramp). See Methods and SI.

Figure 2 Demonstration of sub-diffraction optical spin imaging. **a**, Scanning 1D optical images of an NV electronic spin in diamond, for several values of doughnut pulse duration (t_D) at 2 mW total doughnut beam power. Contrast is defined as the number of readout

counts during the reference readout (period B in Figure 1) minus the number of counts during signal (period A). **b**, Resolution (FWHM) of 1D spin images as a function of doughnut pulse duration, for both 2 mW and 0.1 mW total doughnut beam power. The error bars represent 95% confidence intervals. Solid lines represent a fit to Equation (1). Equivalent resolution is achieved for lower power optical fields applied for longer duration. Long NV spin lifetimes ($>$10 ms) enables comparable resolution for the present spin-RESOLFT technique with $\sim$0.1$\%$ of the laser power used in STED imaging of NV centers [23]. Resolution is limited by imperfections of the doughnut intensity zero, and/or mechanical instability during doughnut application, which leads to loss of contrast for very large t_D (inset).

Figure 3 Sub-diffraction optical magnetic sensing. **a**, Multiple NV centers cannot be identified or distinguished by their optically-detected ESR spectrum, acquired using confocal fluorescence microscopy. **b**, Confocal image does not resolve multiple NV centers; whereas 2D spin imaging using spin-RESOLFT reveals two NV centers separated by $\sim$150 nm. The image has 50 x 50 pixels, with a data acquisition time per pixel of 7.2 seconds. **c**, spin-RESOLFT provides spatially-selective measurements of Rabi oscillations for the two neighboring NV spins, which display stark differences due to different local magnetic field environments. **d**, spin-RESOLFT also enables spatially-selective spin-echo measurements for the two NV spins, which reveal substantial differences in spin coherence times, indicating the presence of magnetic impurities in the local environment of NV Center 1. Solid lines in **c** and **d** are fits to a model that includes the electronic spin of the NV center and the nuclear spin of the center's ^{15}N atom.

Figure 4 Sub-diffraction coherent manipulation of spectrally indistinguishable NV spins using optically-induced effects. **a**, Suppression of a single, isolated NV center's spin transitions, driven by a resonant microwave pulse, as a function of Gaussian laser beam power (characterized by the NV optical excitation rate, κ). Using sequences S1 and S2, the populations of the $m_s = 0$ state (red), $m_s = +1$ state (green), and $^1A_1$ state (blue) were measured with (triangles) and without (open circles) a resonant microwave π pulse of 130 ns duration, applied simultaneously with the Gaussian optical beam. The state populations were determined by recording the fluorescence right after microwave pulse application ($\tau_d < 50$ ns) and also after waiting for a time ($\tau_d = 5$ μs) much longer than the singlet deshelving time (300 ns). The comparison between these two measurements allows us to extract the populations of all states, including the singlet (see SI). Solid lines are fits using the master equation described in Ref. [32] and in the SI. **b**, Coherent spin transitions induced by resonant microwave radiation (MW) are inhibited for NV centers away from the central null of a simultaneously applied green doughnut beam. Selective Rabi oscillations are observed only for the NV spin in the doughnut null (Center 1); whereas NV Center 2, separated from Center 1 by 150 nm, is located outside the doughnut null, and is observed to remain in the ground state. Populations of Centers 1 and 2 are obtained from experimental sequences S3 and S4 as described in SI.

a

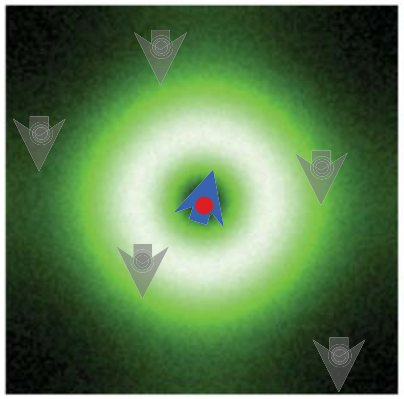

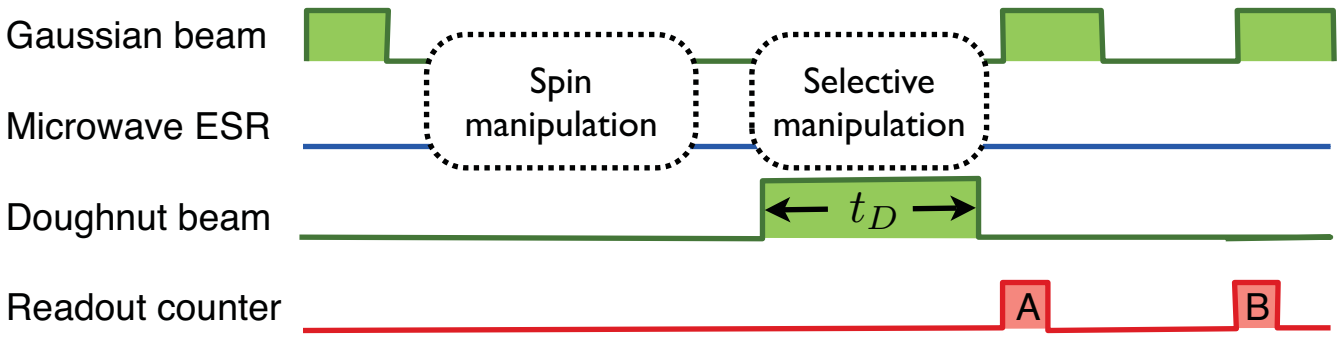
Gaussian beam
Microwave ESR
Doughnut beam
Readout counter
Spin manipulation
Selective manipulation
t_D
A
B

b

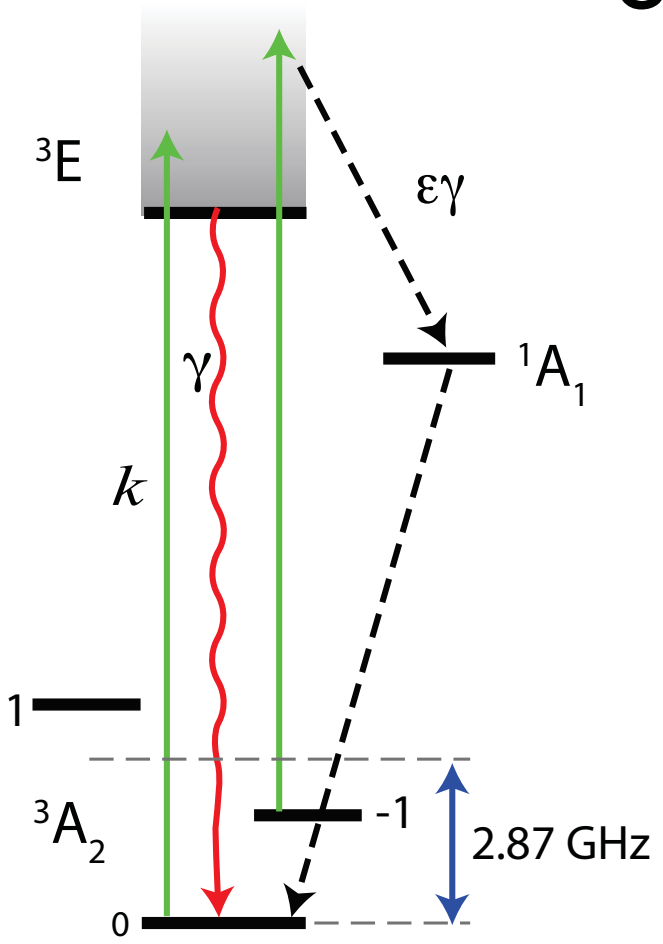
^{3}E
εγ
γ
^{1}A$_1$
k
1
^{3}A$_2$
-1
0
2.87 GHz

c

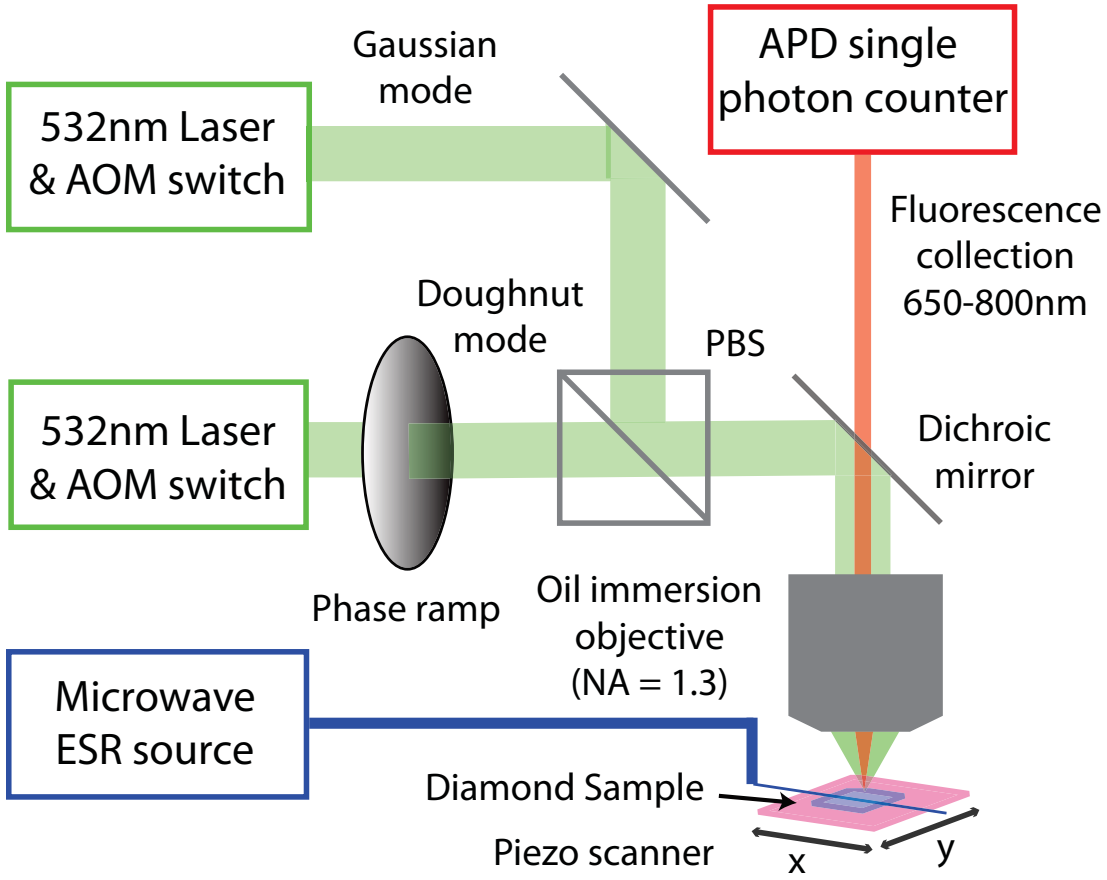
Gaussian mode
APD single photon counter
532nm Laser & AOM switch
Fluorescence collection 650-800nm
Doughnut mode
PBS
532nm Laser & AOM switch
Dichroic mirror
Phase ramp
Oil immersion objective (NA = 1.3)
Microwave ESR source
Diamond Sample
Piezo scanner
x
y

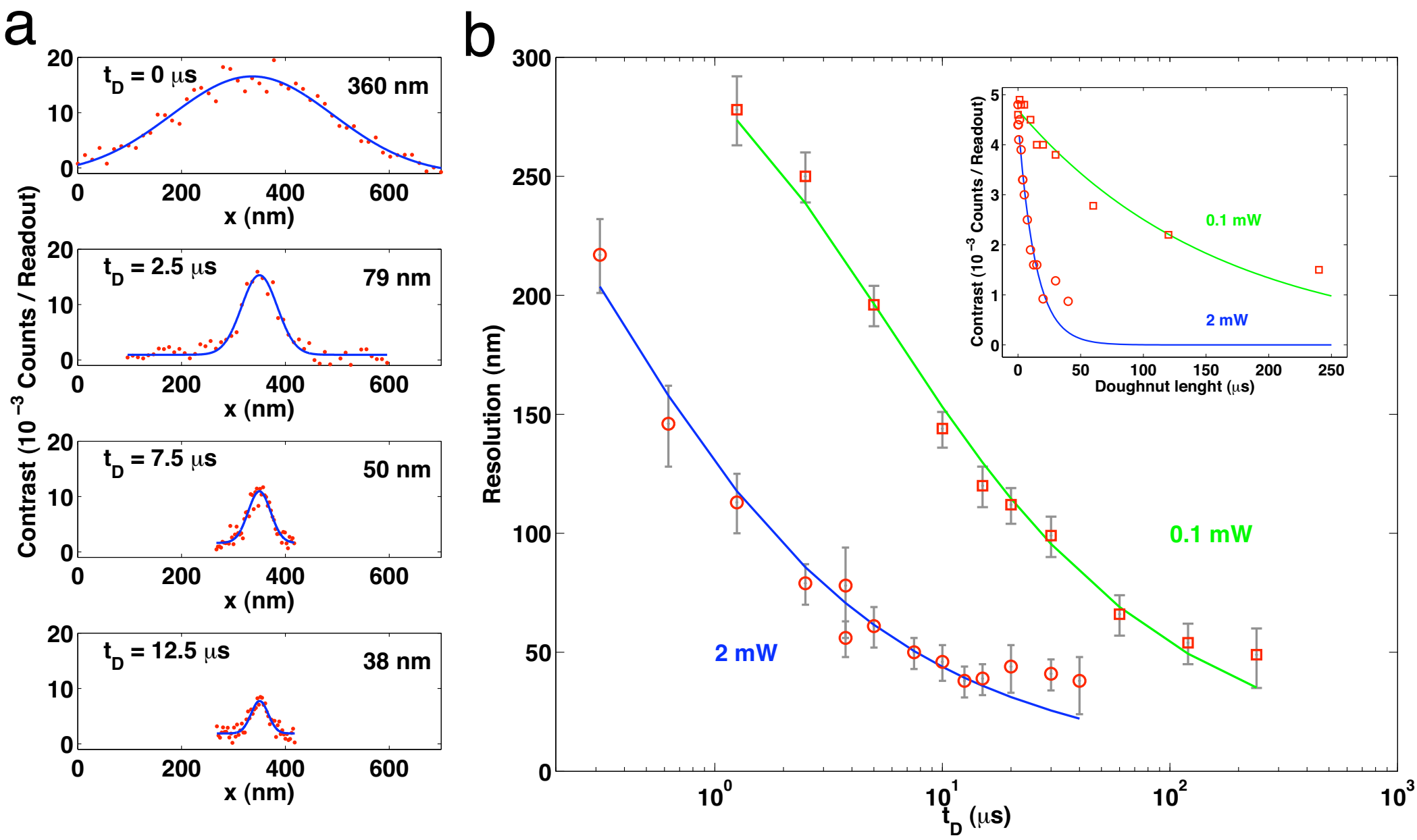
a
b
t_D = 0 μs
360 nm
t_D = 2.5 μs
79 nm
t_D = 7.5 μs
50 nm
t_D = 12.5 μs
38 nm
x (nm)
Contrast (10^{-3} Counts / Readout)
Resolution (nm)
t_D (μs)
0.1 mW
2 mW
Doughnut lenght (μs)

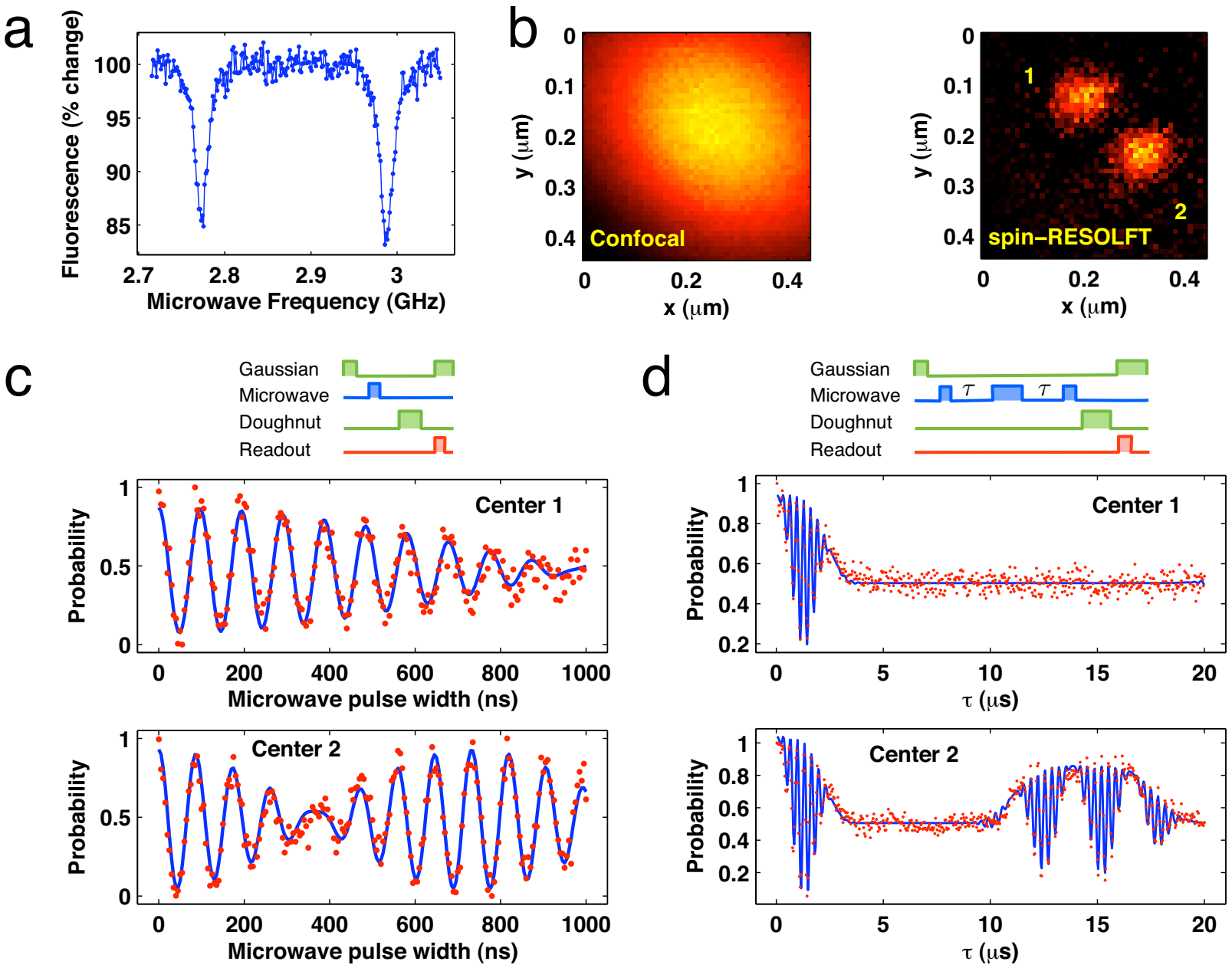
a
Fluorescence (% change)
100
95
90
85
2.7
2.8
2.9
3
Microwave Frequency (GHz)
b
y (μm)
0
0.1
0.2
0.3
0.4
Confocal
0
0.2
0.4
x (μm)
1
2
spin–RESOLFT
c
Gaussian
Microwave
Doughnut
Readout
Probability
Center 1
Microwave pulse width (ns)
Center 2
d
τ
τ (μs)

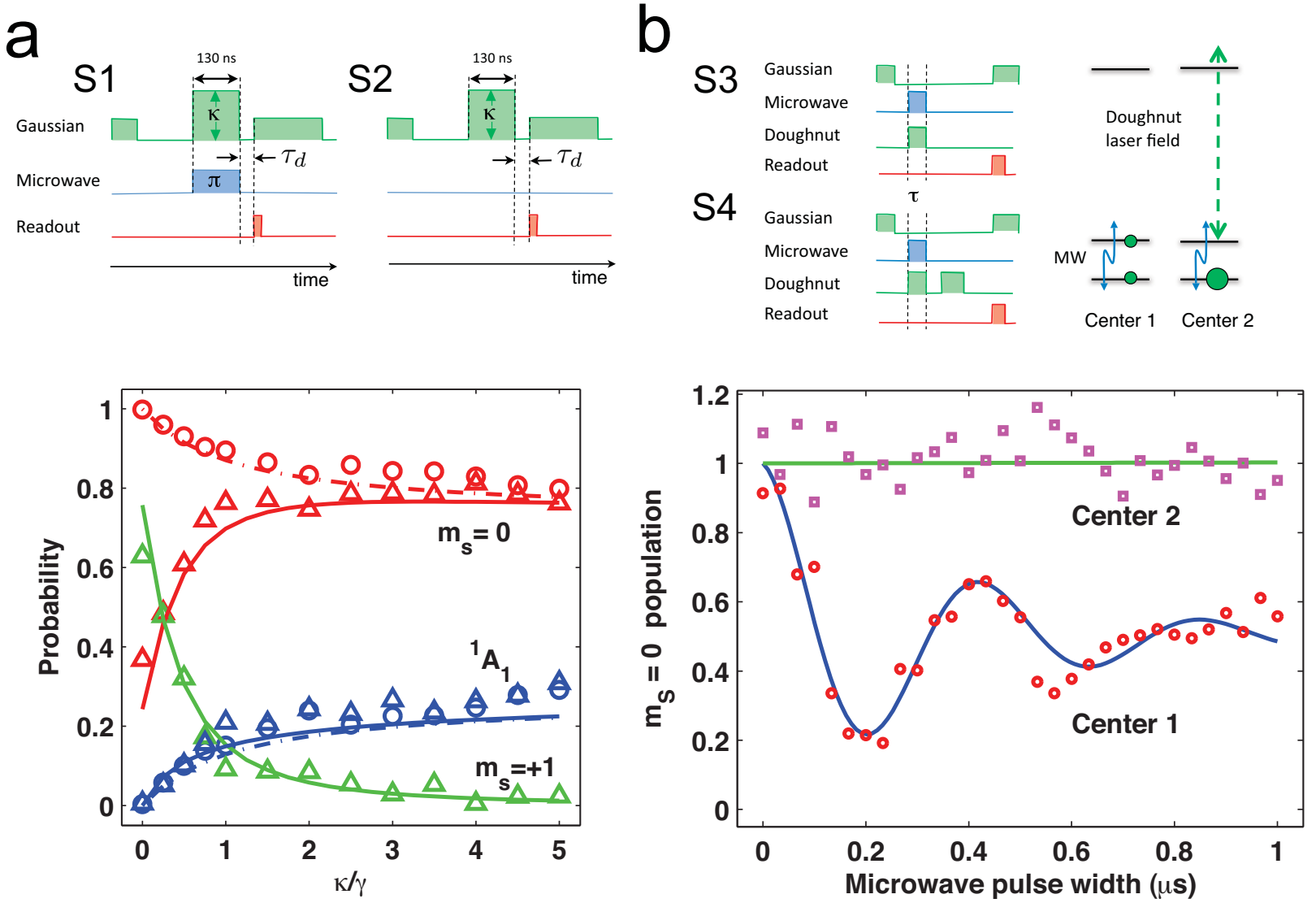
a
S1
130 ns
κ
Gaussian
Microwave
π
τ_d
Readout
time
S2
130 ns
κ
τ_d
time
b
S3
Gaussian
Microwave
Doughnut
Readout
τ
S4
Gaussian
Microwave
Doughnut
Readout
Doughnut
laser field
MW
Center 1
Center 2
Probability
m_s= 0
$^1A_1$
m_s=+1
κ/γ
m_S = 0 population
Center 2
Center 1
Microwave pulse width (μs)